Low-lying states of odd-even $N = 79$ isotones within the nucleon-pair approximation*

Yu-Chen Wu (吴雨晨)[1] Man Bao (鲍曼)[1†]

[1]Department of Physics, University of Shanghai for Science and Technology, Shanghai 200093, China

Abstract: In this paper, we study low-lying states of odd-even $N = 79$ isotones, including ^{129}Sn, ^{131}Te, ^{133}Xe, ^{135}Ba, and ^{137}Ce, within the nucleon-pair approximation (NPA) of the shell model. Low-lying energy levels of these nuclei with both positive and negative parities, as well as $B(E2)$ transition rates and g factors of some low-lying states, are calculated. Most of them agree closely with experimental data. The wave functions of yrast $1/2^+_1$, $5/2^+_1$, $7/2^+_1$, $23/2^+_1$ states and negative parity $11/2^-_1 \sim 23/2^-_1$ and $27/2^-_2$ states of these nuclei are discussed in detail. The NPA calculations show that many of these states have a simple structure in the nucleon-pair basis.

Keywords: nucleon-pair approximation, low-lying states, wave functions

DOI: 10.1088/1674-1137/adf1f6 **CSTR:** 32044.14.ChinesePhysicsC.49124109

I. INTRODUCTION

The structure of nuclei with the mass number A around 130 has been a focal point of research in both nuclear physics and astrophysics. Interesting features such as the back-bending phenomenon, high-spin isomers, and γ instability in low-lying states for nuclei in this region have attracted much interest in recent years, and many results have been achieved [1−10]. Here, odd-mass nuclei with the neutron number $N = 79$ exhibit a competition between the evolution of nuclear collectivity and the excitation of single-particle states, and the neutron $h_{11/2}$ orbit plays a pivotal role in generating high-spin states. The isomeric $11/2^-_1$ states with neutron-hole configurations $\nu h^{-1}_{11/2}$ have been discovered in all odd-mass $N = 79$ isotones, and several high-spin isomers above this $11/2^-_1$ state have been reported [11].

A fundamental framework for describing nuclei with $A \sim 130$ is the nuclear shell model (NSM) [12−17]. However, the configuration truncation is indispensable owing to the explosively increased configuration space of the NSM. The nucleon-pair approximation (NPA) [18−21] is one of the practical approaches and has been proved to be effective in studying the low-lying states of nuclei in this region [21−28]. For odd-mass $N = 79$ isotones, the NPA with only S and D pairs (spin equals 0 and 2) can describe the yrast states and some negative parity states below 1 MeV [24]. For higher states, pairs with higher spin should be considered.

Recently, the NPA with high-spin pairs, neutron $(h_{11/2})^{-2}$ configuration, and several nucleon pairs with negative parity have been employed to investigate isotones with $N = 80$ [27]. Most calculated energy levels, $B(E2)$ transition rates, and g factors of the low-lying states of ^{130}Sn, ^{132}Te, ^{134}Xe, ^{136}Ba, and ^{138}Ce are consistent with experimental values. This paper extends the approach to study the low-lying states of $N = 79$ isotones, *i.e.*, ^{129}Sn, ^{131}Te, ^{133}Xe, ^{135}Ba, and ^{137}Ce, and discusses the wave functions of some low-lying states in detail.

The remainder of this paper is organized as follows. In Sec. II, a brief introduction to the formulation of the NPA is given, including the phenomenological Hamiltonian, nucleon-pair basis states, and electromagnetic-transition operators. The calculated results are given and discussed in Sec. III, and the summary is provided in Sec. IV. Analytical matrix elements of two-body interaction operators for odd system with one nucleon-pair are presented in Appendix A.

II. THEORETICAL FRAMEWORK

In this section, we briefly introduce the NPA, which was first developed by Chen [29] and was generalized and refined in Refs. [30−33]. In our calculations, we only consider the $50 \sim 82$ major shell with five single-particle(-hole) orbits: $0g_{7/2}$, $1d_{5/2}$, $1d_{3/2}$, $2s_{1/2}$, and $0h_{11/2}$.

Received 24 April 2025; Accepted 21 July 2025; Published online 22 July 2025

* Supported by National Natural Science Foundation of China (11905130)

† E-mail: mbao@usst.edu.cn

A. Hamiltonian

The Hamiltonian in this paper is similar to that in Ref. [27] and includes the spherical single-particle(-hole) energy H_0, residual interactions between the like valence particles H_P, and quadrupole-quadrupole interactions between all valence particles H_Q, *i.e.*,

$$H = H_0 + H_P + H_Q. \tag{1}$$

The first term H_0 is defined as

$$H_0 = \sum_{\alpha\sigma} \epsilon_{\alpha\sigma} C^\dagger_{\alpha\sigma} C_{\alpha\sigma}, \tag{2}$$

where $C^\dagger_{\alpha\sigma}$ ($C_{\alpha\sigma}$) is a creation (an annihilation) operator, with $\alpha = (nljm)$ denoting all the quantum numbers required for a nucleus and $\sigma = \pi$ or ν corresponding to the proton or neutron degrees of freedom. The single-particle(-hole) energies of valence protons $\epsilon_{j\pi}$ (valence neutron holes $\epsilon_{j\nu}$) tabulated in Table 1 are obtained from experimental energies of the lowest states with spin j in ^{133}Sb (^{131}Sn) [34–36], except $\epsilon_{j\nu}$ for $1/2^+$, which increases by 0.1 MeV, and for $11/2^-$, which equals $0.02+0.01N_\pi$ (N_π is the valence proton number). This adjustment is similar to those in Refs. [7, 9] and is primarily performed to reproduce the energy levels of low-lying states.

The second term in Eq. (1), H_P, is defined as

$$H_P = V_0 + V_2 + V_4 + V_{10}, \tag{3}$$

where

$$\begin{aligned} V_0 &= G^{(0)}_\pi \mathcal{P}^{(0)\dagger}_\pi \cdot \widetilde{\mathcal{P}}^{(0)}_\pi + G^{(0)}_\nu \mathcal{P}^{(0)\dagger}_\nu \cdot \widetilde{\mathcal{P}}^{(0)}_\nu, \\ V_2 &= G^{(2)}_\pi \mathcal{P}^{(2)\dagger}_\pi \cdot \widetilde{\mathcal{P}}^{(2)}_\pi + G^{(2)}_\nu \mathcal{P}^{(2)\dagger}_\nu \cdot \widetilde{\mathcal{P}}^{(2)}_\nu, \\ V_4 &= G^{(4)}_\pi \mathcal{P}^{(4)\dagger}_\pi \cdot \widetilde{\mathcal{P}}^{(4)}_\pi + G^{(4)}_\nu \mathcal{P}^{(4)\dagger}_\nu \cdot \widetilde{\mathcal{P}}^{(4)}_\nu, \\ V_{10} &= G^{(10)}_\nu \mathcal{P}^{(10)\dagger}_\nu \cdot \widetilde{\mathcal{P}}^{(10)}_\nu. \end{aligned} \tag{4}$$

Here, the interaction parameters $G^{(t)}_\sigma$ ($t = 0, 2, 4, 10$) of ^{129}Sn, ^{131}Te, ^{133}Xe, ^{135}Ba, and ^{137}Ce are tabulated in Table 2. For $t = 0$,

$$\begin{aligned} \mathcal{P}^{(0)\dagger}_\sigma &= \sum_{a_\sigma} \frac{\sqrt{2j_\sigma + 1}}{2} (C^\dagger_{a_\sigma} \times C^\dagger_{a_\sigma})^{(0)}_0, \\ \widetilde{\mathcal{P}}^{(0)}_\sigma &= -\sum_{a_\sigma} \frac{\sqrt{2j_\sigma + 1}}{2} (\widetilde{C}_{a_\sigma} \times \widetilde{C}_{a_\sigma})^{(0)}_0. \end{aligned} \tag{5}$$

For $t = 2$ and 4,

$$\begin{aligned} \mathcal{P}^{(t)\dagger}_{\sigma M} &= \sum_{a_\sigma b_\sigma} q(a_\sigma b_\sigma t)(C^\dagger_{a_\sigma} \times C^\dagger_{b_\sigma})^{(t)}_M, \\ \widetilde{\mathcal{P}}^{(t)}_{\sigma M} &= -\sum_{a_\sigma b_\sigma} q(a_\sigma b_\sigma t)(\widetilde{C}_{a_\sigma} \times \widetilde{C}_{b_\sigma})^{(t)}_M, \end{aligned} \tag{6}$$

Table 1. Single-particle(-hole) energies (in MeV) of valence protons (valence neutron holes) obtaineed from yrast state energies of ^{133}Sb (^{131}Sn) [34–36], except $\epsilon_{j\nu}$ for $1/2^+$ ($11/2^-$), which increases by 0.1 MeV (equals ϵ). Here, $\epsilon = 0.02 + 0.01N_\pi$.

j^{parity}	$1/2^+$	$3/2^+$	$5/2^+$	$7/2^+$	$11/2^-$
$\epsilon_{j\pi}$	2.990	2.690	0.963	0.000	2.760
$\epsilon_{j\nu}$	0.432	0.000	1.655	2.434	ϵ

where

$$q(ab\lambda) = -\frac{1}{\sqrt{2\lambda+1}} \frac{\langle j_a \| r^\lambda Y^\lambda \| j_b \rangle}{r_0^\lambda} \tag{7}$$

and r_0 is the oscillator parameter ($r_0^2 = 1.012A^{1/3}$ fm^2). For $t = 10$,

$$\mathcal{P}^{(10)\dagger}_\nu = (C^\dagger_j \times C^\dagger_j)^{(10)}_M, \quad \widetilde{\mathcal{P}}^{(10)}_\nu = -(\widetilde{C}_j \times \widetilde{C}_j)^{(10)}_M, \tag{8}$$

where j corresponds to the neutron $h_{11/2}$ orbit.

The last term in Eq. (1) is H_Q, which is the sum of the quadrupole-quadrupole interaction between the like valence nucleons V_Q and proton-neutron interaction $V_{Q_{\pi\nu}}$. Here,

$$V_Q = \sum_\sigma \kappa^{(2)}_\sigma Q^{(2)}_\sigma \cdot Q^{(2)}_\sigma, \tag{9}$$

$$V_{Q_{\pi\nu}} = \kappa Q^{(2)}_\pi \cdot Q^{(2)}_\nu, \tag{10}$$

with the operator

$$Q^{(2)}_{\sigma M} = \sum_{ab} q(ab2)(C^\dagger_{a_\sigma} \times \widetilde{C}_{b_\sigma})^{(2)}_M, \tag{11}$$

and interaction parameters $\kappa^{(2)}_\sigma$ and κ are also given in Table 2.

B. Configuration basis

With the convention $\widetilde{C}_{jm} = (-1)^{j-m} C_{j-m}$, a non-collective nucleon pair with spin r and projection μ, as well as its time reversal, can be defined as

$$\begin{aligned} A^r_\mu(ab)^\dagger &= (C^\dagger_a \times C^\dagger_b)^{(r)}_\mu, \\ \widetilde{A}^r_\mu(ab) &= -(\widetilde{C}_a \times \widetilde{C}_b)^{(r)}_\mu, \end{aligned} \tag{12}$$

where a and b are the angular momenta of single-particle orbits. A collective nucleon pair and its time reversal can be defined as

Table 2. Interaction parameters of ^{129}Sn, ^{131}Te, ^{133}Xe, ^{135}Ba, and ^{137}Ce. $G_\nu^{(0)}$, $G_\pi^{(0)}$, and $G_\nu^{(10)}$ are in units of MeV, $G_\nu^{(4)}$ is in units of MeV/r_0^8, and the others are in units of MeV/r_0^4. A smooth change in these parameters with the valence proton number N_π is assumed.

$G_\nu^{(0)}$	$G_\nu^{(2)}$	$G_\nu^{(4)}$	$G_\nu^{(10)}$	$\kappa_\nu^{(2)}$
$-0.155-0.0015N_\pi$	$-0.019-0.00025N_\pi$	$-0.0001-0.000035N_\pi$	$0.15+0.04N_\pi$	$-0.030+0.002N_\pi$
$G_\pi^{(0)}$	$G_\pi^{(2)}$	$G_\pi^{(4)}$	$\kappa_\pi^{(2)}$	κ
$-0.213+0.0015N_\pi$	$-0.029+0.0015N_\pi$	$-0.00105+0.00005N_\pi$	$-0.070+0.005N_\pi$	$0.070+0.005N_\pi$

$$A_\mu^{r\dagger}=\sum_{ab}y(abr)(C_a^\dagger\times C_b^\dagger)_\mu^{(r)},$$
$$\widetilde{A}_\mu^{r}=-\sum_{ab}y(abr)(\widetilde{C}_a\times\widetilde{C}_b)_\mu^{(r)}, \quad (13)$$

where the structure coefficients $y(abr)$ of the collective pair satisfy the symmetry

$$y(abr)=(-1)^{a+b+r+1}y(bar) \quad (14)$$

and are obtained using the procedure given in Ref. [37].

For an odd system with $2n+1$ nucleons, the NPA basis state can be constructed by coupling n nucleon pairs and an unpaired nucleon in the j-orbit, *i.e.*,

$$|\tau J_n M_n\rangle\equiv A_{M_n}^{J_n\dagger}(r_0r_1\cdots r_n,J_1J_2\cdots J_n)|0\rangle$$
$$=\{\cdots[(C_j^\dagger\times A^{r_1\dagger})^{(J_1)}\times A^{r_2\dagger}]^{(J_2)}\times\cdots\times A^{r_n\dagger}\}_{M_n}^{(J_n)}|0\rangle, \quad (15)$$

where J_n and M_n are the total angular momentum and its projection of these $2n+1$ nucleons, respectively, and τ represents additional necessary quantum numbers.

In this paper, S,D,F,G,H,I, and $\mathcal{J}$ are used to represent a nucleon pair with spin 0, 2, 3, 4, 5, 6, and 7, respectively. Similar to Ref. [27], collective S^+,D^+,G^+,I^+ pairs are used to construct the proton nucleon-pair basis states, expect for ^{137}Ce for which collective S^+,D^+ pairs and up to one G^+ pair and one I^+ pair are considered owing to the computational cost; collective S^+,S'^+ (second spin-zero), D^+,G^+, and $F^-,G^-,H^-,I^-,\mathcal{J}^-$ pairs, as well as non-collective $(\nu h_{11/2})^{-2}$ pairs (denoted by $\mathcal{A}_\nu^{(J)}$ with $J=2,4,6,8,10$) are taken to construct the neutron nucleon-pair basis states. The basis states in this paper are normalized but non-orthogonal to each other.

C. Electromagnetic-transition operators

The $E2$ transition operator in this paper is defined as

$$T(E2)=\sum_\sigma e_\sigma r_\sigma^2 Y_\sigma^2, \quad (16)$$

where $e_\sigma(\sigma=\pi,\nu)$denotes the effective charges (including bare charges) of valence protons and valence neutron holes. The $M1$ transition operator is defined as

$$T(M1)=\sqrt{\frac{3}{4\pi}}\hat{\mu}=\sqrt{\frac{3}{4\pi}}\sum_\sigma(g_{l\sigma}\vec{L}_\sigma+g_{s\sigma}\vec{S}_\sigma), \quad (17)$$

where $g_{l\sigma}$ ($g_{s\sigma}$) is the orbital (spin) gyromagnetic ratios, and L_σ (S_σ) is the total orbital angular momentum (total spin) operator. The g factor is defined as μ/J (J is the total angular momentum), with

$$\mu=\langle\Psi_{JM}|\hat{\mu}_z|\Psi_{JM}\rangle_{M=J}. \quad (18)$$

Similar to Ref. [27], we set $e_\pi=1.79$; $e_\nu=-0.71$ (in units of e); and $g_{l\pi}=1.00$, $g_{l\nu}=0.02$, $g_{s\pi}=5.586\times0.7$, $g_{s\nu}=-3.826\times0.7$ (in unit of $\mu_N/\hbar$). Here, the sign of e_ν is negative because we use the hole-like picture.

III. RESULTS AND DISCUSSIONS

In this section, our calculated results of ^{129}Sn, ^{131}Te, ^{133}Xe, ^{135}Ba, and ^{137}Ce are presented and discussed. Figure 1 and Fig. 2 present the calculated energy levels for these five $N=79$ isotones, comparing them with experimental values obtained from Ref. [36]. The energy levels of most low-lying states are well reproduced. Some energy levels for which the experimental results remain inconclusive are also plotted. In addition, our calculated $B(E2)$ transition rates (in units of W.u.) and g factors (in

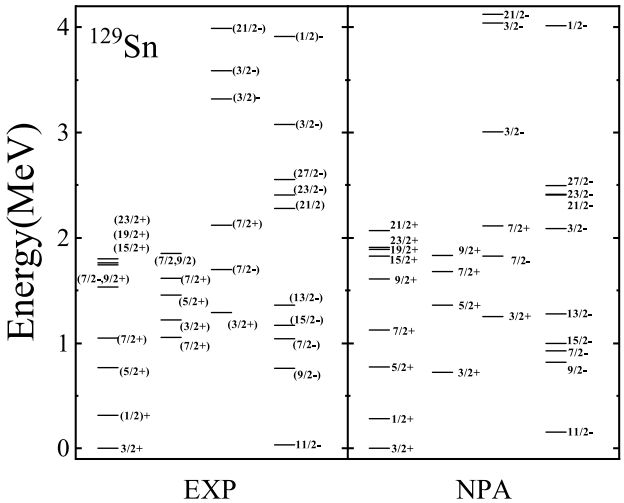

Fig. 1. Energy levels of ^{129}Sn. The left-hand (right-hand) side corresponds to experimental values [36] (our NPA calculated results).

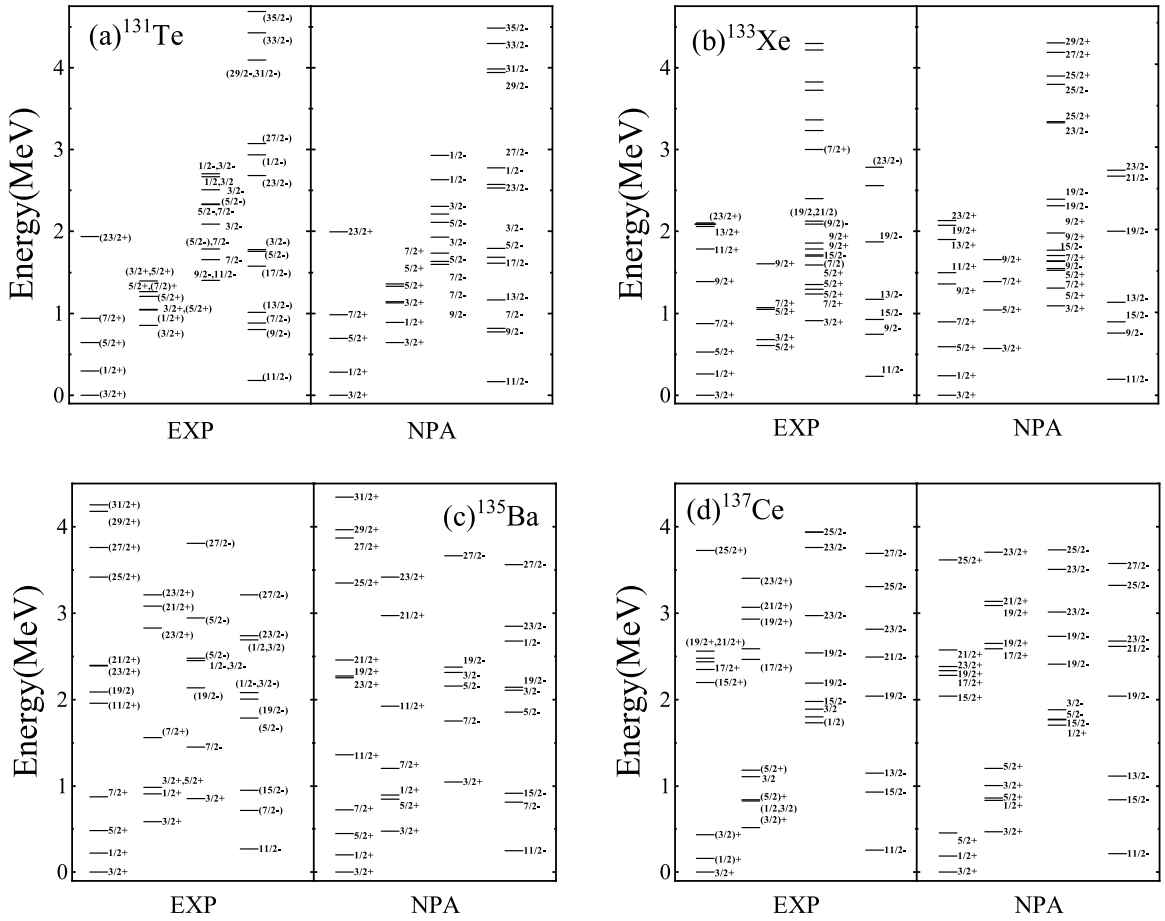

Fig. 2. Same as Fig. 1. Panels (a), (b), (c), and (d) correspond to ^{131}Te, ^{133}Xe, ^{135}Ba, and ^{137}Ce, respectively.

units of μ_N) for low-lying states are presented in Table 3 and Table 4, respectively. The corresponding experimental values [36] and some other calculations of $B(E2)$ [3, 9, 28, 38, 39] and g factors [9, 24, 28, 40, 41] are also given for comparison. Our calculated $B(E2)$ and g factors show reasonable agreement with experimental values.

A. ^{129}Sn

Let us begin the discussion with ^{129}Sn, a nucleus with only three valence neutron holes. As shown in Fig. 1, the energy levels of most low-lying states are well reproduced except for the $7/2^+_2$ state, which exhibits a significant deviation from the experimental value. The same deviations can also be observed in Refs. [42−44]. Experimentally, energies of the first two probable $7/2^+$ states are very close (1.047 and 1.054 MeV). Therefore, the calculated $7/2^+_2$ state may correspond to the $7/2^+$ state at 1.865 MeV observed experimentally, as their energies are comparable (see Fig. 1).

For the wave functions of low-lying states of ^{129}Sn, the dominant components of the $11/2^-_1$ state are $\nu h^{-3}_{11/2}$ and $\nu h^{-1}_{11/2}d^{-2}_{3/2}$ [39, 43, 45], and those of the $3/2^+_2$, $5/2^+_1$, $7/2^+_1$ states are the $d_{3/2}$ neutron holes [44]. Reference [46] also indicates that one of the three neutron holes always occupies the $s_{1/2}$ orbit for the $1/2^+_1$ state. The NSM calculation produces 39% $\nu h^{-3}_{11/2}$ and 34% $\nu h^{-1}_{11/2}d^{-2}_{3/2}$ components of the $11/2^-_1$ state and 57% $\nu h^{-2}_{11/2}s^{-1}_{1/2}$ and 27% $\nu d^{-2}_{3/2}s^{-1}_{1/2}$ components of the $1/2^+_1$ state [39]. In our NPA calculations, the wave function of the $11/2^-_1$ state for ^{129}Sn is

$$|11/2^-_1\rangle = -0.99|S^+_\nu \otimes \nu h^{-1}_{11/2}\rangle + \cdots, \tag{19}$$

which contains about 58% $\nu h^{-3}_{11/2}$ and 34% $\nu h^{-1}_{11/2}d^{-2}_{3/2}$ components, and that of the$1/2^+_1$ state is

$$|1/2^+_1\rangle = -0.99|S^+_\nu \otimes \nu s^{-1}_{1/2}\rangle + \cdots, \tag{20}$$

which contains about 44% $\nu h^{-2}_{11/2}s^{-1}_{1/2}$ and 24% $\nu d^{-2}_{3/2}s^{-1}_{1/2}$ components, and those of the $3/2^+_2$, $5/2^+_1$ and $7/2^+_1$ states are

$$\begin{aligned}
|3/2^+_2\rangle &= -0.91|D^+_\nu \otimes \nu d^{-1}_{3/2}\rangle + \cdots, \\
|5/2^+_1\rangle &= -0.97|D^+_\nu \otimes \nu d^{-1}_{3/2}\rangle + \cdots, \\
|7/2^+_1\rangle &= 0.94|D^+_\nu \otimes \nu d^{-1}_{3/2}\rangle + \cdots,
\end{aligned} \tag{21}$$

Table 3. $B(E2)$ values (in units of W.u.) of ^{129}Sn, ^{131}Te, ^{133}Xe, ^{135}Ba, and ^{137}Ce. Some experimental values [36] and theoretical results obtained from [a]Ref. [9], [b]Ref. [39], [c]Ref. [38], [d]Ref. [28], and [e]Ref. [3] are also given for comparison.

	$J_i \to J_f$	$B(E2)$		
		NPA	Others	Expt.
^{129}Sn	$3/2^+_1 \to 1/2^+_1$	0.758	1.11[a]	–
	$5/2^+_1 \to 3/2^+_1$	1.54	1.88[a]	–
	$5/2^+_1 \to 1/2^+_1$	0.272	0.0328[a]	–
	$19/2^+_1 \to 15/2^+_1$	1.38	1.39[a]/0.83[b]	1.4(6)
	$23/2^+_1 \to 19/2^+_1$	0.829	0.633[a]/0.58[b]	1.39(10)
	$9/2^-_1 \to 11/2^-_1$	1.87	3.02[a]	–
	$7/2^-_1 \to 11/2^-_1$	1.72	1.97[a]	–
	$7/2^-_1 \to 9/2^-_1$	1.01	0.169[a]	–
	$15/2^-_1 \to 11/2^-_1$	1.69	0.97[b]	1.12(34)
	$27/2^-_1 \to 23/2^-_1$	0.561	0.565[c]	0.79(36)
^{131}Te	$1/2^+_1 \to 3/2^+_1$	2.63	8.23[a]	–
	$5/2^+_1 \to 3/2^+_1$	5.97	7.92[a]	–
	$5/2^+_1 \to 1/2^+_1$	0.739	0.0212[a]	–
	$7/2^+_1 \to 3/2^+_1$	6.20	8.40[a]	10.17[d]
	$9/2^-_1 \to 11/2^-_1$	6.19	8.99[a]	–
	$7/2^-_1 \to 9/2^-_1$	3.46	1.25[a]	–
	$7/2^-_1 \to 11/2^-_1$	6.95	7.83[a]	–
	$15/2^-_1 \to 11/2^-_1$	7.11	12.70[d]	–
	$13/2^-_1 \to 11/2^-_1$	7.6	8.125[e]	–
	$17/2^-_1 \to 13/2^-_1$	2.95	3.07[a]/2.37[d]/2.255[e]	3.5
	$19/2^-_1 \to 15/2^-_1$	5.51	4.24[d]	–
	$23/2^-_1 \to 19/2^-_1$	7.69	1.88[d]	–
^{133}Xe	$1/2^+_1 \to 3/2^+_1$	6.04	15.1[a]	–
	$5/2^+_1 \to 3/2^+_1$	13.74	19.9[a]	–
	$7/2^+_1 \to 3/2^+_1$	11.81	17.5[a]	–
	$9/2^-_1 \to 11/2^-_1$	10.9	15.2[a]	–
	$15/2^-_1 \to 11/2^-_1$	10.6	13.8[a]	–
^{135}Ba	$1/2^+_1 \to 3/2^+_1$	11.7	16.2[a]	4.6(2)
	$1/2^+_2 \to 3/2^+_1$	6.43	2.21[a]	11.7(10)
	$3/2^+_2 \to 3/2^+_1$	17.04	10.9[a]	18(10)
	$5/2^+_1 \to 1/2^+_1$	2.55	1.31[a]	2.6(5)
	$5/2^+_1 \to 3/2^+_1$	30.63	37.2[a]	28.3(10)
	$7/2^+_1 \to 3/2^+_1$	21.5	25.0[a]	19.9(8)
^{137}Ce	$1/2^+_1 \to 3/2^+_1$	12.46	–	–
	$3/2^+_2 \to 3/2^+_1$	18.16	–	–
	$15/2^-_1 \to 11/2^-_1$	16.98	–	–
	$9/2^-_1 \to 11/2^-_1$	15.83	–	–
	$9/2^-_1 \to 7/2^-_1$	12.04	–	–
	$13/2^-_1 \to 9/2^-_1$	0.214	–	–

Table 4. g factors (in units of μ_N) of ^{129}Sn, ^{131}Te, ^{133}Xe, ^{135}Ba, and ^{137}Ce. Some experimental values [36] and theoretical results taken from [a]Ref. [9], [b]Ref. [41], [c]Ref. [24], [d]Ref. [28], and [e]Ref. [40] are also given for comparison.

	J	g factor		
		NPA	Others	Expt.
^{129}Sn	$3/2^+_1$	0.806	0.803[a]/0.817[b]/0.761[c]	0.754(6)
	$1/2^+_1$	−1.234	−1.250[c]	–
	$5/2^+_1$	0.129	0.116[a]/0.06[c]	–
	$7/2^-_1$	−1.134	−0.899[a]	–
	$9/2^-_1$	−1.067	−1.11[a]/−1.152[c]	–
	$11/2^-_1$	−1.238	−1.34[a]/−1.264[b]/−1.337[c]	−1.297(5)
^{131}Te	$3/2^+_1$	0.833	0.843[a]/0.773[c]	0.696(9)
	$1/2^+_1$	−1.21	−1.200[c]	–
	$5/2^+_1$	0.358	0.356[a]/0.463[c]	–
	$7/2^+_1$	1.05	0.835[a]	–
	$7/2^-_1$	−1.29	−1.39[a]	–
	$9/2^-_1$	−1.07	−1.11[a]/−1.22[c]	–
	$11/2^-_1$	−1.21	−1.30[a]/−1.32[c]	−1.04(4)
	$15/2^-_1$	−0.902	−0.66[d]	–
	$19/2^-_1$	1.78	2.31[d]	–
	$23/2^-_1$	2.20	3.41[d]	–
	$17/2^-_1$	1.64	2.34[d]	–
^{133}Xe	$3/2^+_1$	0.87	0.892[a]/0.782[c]	0.8134(7)
	$1/2^+_1$	−1.185	−1.14[c]	–
	$5/2^+_1$	0.517	0.651[a]/0.653[c]	–
	$9/2^-_1$	−1.04	−1.10[a]/−1.229[c]	–
	$11/2^-_1$	−1.18	−1.25[a]/−1.298[c]	−1.08247(15)
^{135}Ba	$3/2^+_1$	0.929	0.921[a]/0.790[c]	0.837943(17)
	$1/2^+_1$	−1.111	−1.115[c]	–
	$5/2^+_1$	0.780	0.991[a]/0.723[c]	–
	$7/2^+_1$	1.376	1.530[a]	–
	$9/2^-_1$	−0.971	−1.224[c]	–
	$11/2^-_1$	−1.111	−1.170[a]/−1.287[c]	−1.001(15)
^{137}Ce	$3/2^+_1$	0.947	0.269[e]/0.797[c]	0.96(4)
	$1/2^+_1$	−1.127	−1.085[c]	–
	$5/2^+_1$	0.764	1.020[e]/0.803[c]	–
	$9/2^-_1$	−0.956	−1.06[e]/−1.215[c]	–
	$11/2^-_1$	−1.095	−1.210[e]/−1.276[c]	−1.01(4)

respectively. These calculations agree closely with the results in Refs. [39, 43−46].

For the $15/2^+_1$, $19/2^+_1$, and $23/2^+_1$ states of ^{129}Sn, the dominant configuration is suggested to be $\nu h^{-2}_{11/2} d^{-1}_{3/2}$, whereas for the $23/2^-_1$ and $27/2^-_1$ states, it is suggested to be $\nu h^{-3}_{11/2}$ [38, 39, 44, 47, 48]. The NSM calculation

provides 80% $\nu h^{-2}_{11/2}d^{-1}_{3/2}$ and 16% $\nu h^{-2}_{11/2}s^{-1}_{1/2}$ components of the $19/2^+_1$ state and is similar to the $15/2^+_1$ state [48], whereas they give 97% $\nu h^{-2}_{11/2}d^{-1}_{3/2}$ components of the $23/2^+_1$ state [39] and more than 90% $\nu h^{-3}_{11/2}$ components of the $23/2^-_1$ and $27/2^-_1$ states [38, 48]. In our NPA calculations, about 75%, 81%, and 97% $\nu h^{-2}_{11/2}d^{-1}_{3/2}$ components are obtained in the wave functions of the $15/2^+_1$, $19/2^+_1$, and $23/2^+_1$ states, respectively, and almost 100% $\nu h^{-3}_{11/2}$ components of the $23/2^-_1$ and $27/2^-_1$ states, which agree closely with results in Refs. [38, 39, 44, 47, 48].

B. $1/2^+_1$ states

According to the calculation using the Interacting Boson–Fermion model (IBFM), the ^{131}Te nucleus can be described as consisting of a ^{132}Te core coupled with a neutron hole, and the configuration of the $1/2^+_1$ state is dominated by $\nu s^{-1}_{1/2}$ with a small admixture of $\nu d^{-1}_{3/2}$ [49]. References [50, 51] suggest that the $1/2^+_1$ state of ^{131}Te is identified as a pure single-quasiparticle state. In our NPA calculation, the wave function of the $1/2^+_1$ state for ^{131}Te is

$$\left|1/2^+_1\right\rangle = 0.93|S^+_\pi\rangle\otimes|S^+_\nu\otimes\nu s^{-1}_{1/2}\rangle - 0.33|S^+_\pi\rangle\otimes|D^+_\nu\otimes\nu d^{-1}_{3/2}\rangle + \cdots, \tag{22}$$

which agrees with Refs. [49−51].

Figure 3 presents the overlap squared between excitation configurations and the NPA wave function of the $1/2^+_1$ state for ^{131}Te, ^{133}Xe, ^{135}Ba, and ^{137}Ce versus the mass number A. The red circles and black squares correspond to the $|J_\pi=0\rangle\otimes|S^+_\nu\otimes\nu s^{-1}_{1/2}\rangle$ and $|J_\pi=0\rangle\otimes|D^+_\nu\otimes\nu d^{-1}_{3/2}\rangle$ configurations, respectively. We observe that the configuration $|J_\pi=0\rangle\otimes|S^+_\nu\otimes\nu s^{-1}_{1/2}\rangle$ dominates the $1/2^+_1$ state in these nuclei and decreases with increasing A, whereas the configuration $|J_\pi=0\rangle\otimes|D^+_\nu\otimes\nu d^{-1}_{3/2}\rangle$ increases with A. This is consistent with the experimental energy levels of the $1/2^+_1$ state, which decrease with increasing A, because the single neutron hole energy of $s_{1/2}$ is larger than that of $d_{3/2}$ (see Table 1).

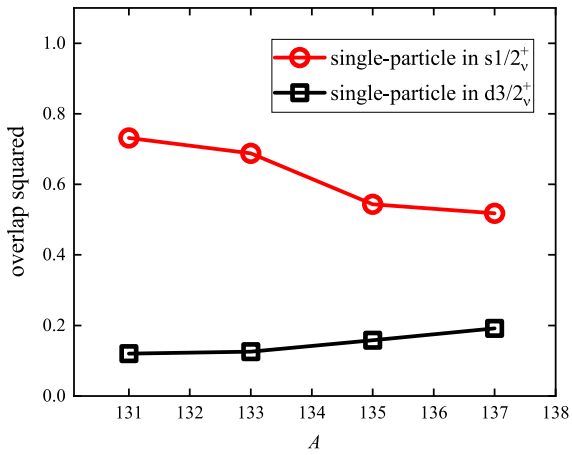

Fig. 3. (color online) Overlap squared between the configurations $|J_\pi=0\rangle\otimes|S^+_\nu\otimes\nu s^{-1}_{1/2}\rangle$ (red circles) and $|J_\pi=0\rangle\otimes|D^+_\nu\otimes\nu d^{-1}_{3/2}\rangle$ (black squares) with the NPA wave function of the $1/2^+_1$ state versus the mass number A.

C. $5/2^+_1$ and $7/2^+_1$ states

Similar to the $1/2^+_1$ state, the $5/2^+_1$ and $7/2^+_1$ states of ^{131}Te are suggested to result essentially from the coupling of quasiparticles to the lowest-lying collective core states, and the configurations of these two states are dominated by $\nu d^{-1}_{3/2}$ [49]. The wave functions of the $5/2^+_1$ and $7/2^+_1$ states for ^{131}Te in our NPA calculations are

$$\begin{aligned}\left|5/2^+_1\right\rangle &= 0.86|S^+_\pi\rangle\otimes|D^+_\nu\otimes\nu d^{-1}_{3/2}\rangle + \cdots,\\ \left|7/2^+_1\right\rangle &= 0.73|S^+_\pi\rangle\otimes|D^+_\nu\otimes\nu d^{-1}_{3/2}\rangle + \cdots,\end{aligned} \tag{23}$$

respectively. Thus, the dominant components of both the $5/2^+_1$ and $7/2^+_1$ states for ^{131}Te are neutron excitations and is consistent with the IBFM results [49].

The orbit with the lowest single-particle energy of valence protons is $g_{7/2}$, and the $h_{11/2}$ orbit has the lowest single-hole energy of valence neutron holes except for the $d_{3/2}$ orbit, which cannot construct a neutron pair with high spin (see Table 1). The percentages of configurations $\pi g^2_{7/2}\otimes\nu h^{-2}_{11/2}d^{-1}_{3/2}$ and $\pi g^2_{7/2}\otimes\nu h^{-2}_{11/2}s^{-1}_{1/2}$ (the single neutron hole is considered to occupy the $d_{3/2}$ or $s_{1/2}$ orbit, which has relatively lower energy and positive parity) in wave functions of positive parity ($1/2^+_1\sim 23/2^+_1$) states for ^{131}Te are calculated and presented in Fig. 4, denoted by solid black squares and red circles, respectively. The corresponding hollow symbols represent results given by the

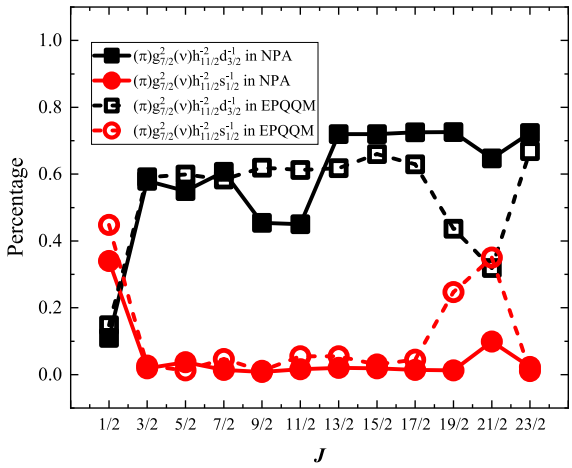

Fig. 4. (color online) Percentages of configurations $\pi g^2_{7/2}\otimes\nu h^{-2}_{11/2}d^{-1}_{3/2}$ (solid black squares) and $\pi g^2_{7/2}\otimes\nu h^{-2}_{11/2}s^{-1}_{1/2}$ (solid red circles) in the NPA wave functions of positive parity states for ^{131}Te versus the angular momentum J. For comparison, the EPQQM results from Ref. [3] are also given, denoted by hollow symbols.

extended pairing plus multipole-multipole force model (EPQQM) [3] and are presented for comparison. The EPQQM is introduced in Ref. [52]. Our calculations show that the configuration $\pi g^2_{7/2}\otimes\nu h^{-2}_{11/2}d^{-1}_{3/2}$ dominates both the $5/2^+_1$ and $7/2^+_1$ states for ^{131}Te, which is in agreement with the results from Ref. [3].

In Fig. 5, the overlap squared between neutron excitation configurations and $|J_\pi = 2\rangle$ configurations with the wave functions of the $5/2^+_1$ and $7/2^+_1$ states is plotted versus the mass number A. The neutron excitation configurations of the $5/2^+_1$ and $7/2^+_1$ states (labeled by red circles and blue triangles) decrease rapidly at ^{133}Xe, whereas $|J_\pi = 2\rangle$configurations (labeled by the black squares and green stars) increase with A. The $5/2^+_1$ and $7/2^+_1$ states of both ^{135}Ba and ^{137}Ce are dominated by $|J_\pi = 2\rangle$ configurations. In addition, owing to the similarity in configurations of these two states for all four nuclei, the calculated $B(E2)$ values of transitions $5/2^+_1 \to 3/2^+_1$ and $7/2^+_1 \to 3/2^+_1$ listed in Table 3 are very close.

D. $23/2^+_1$ states

The $23/2^+_1$ isomer of ^{131}Te is proposed to have a three-quasineutron configuration obtained by coupling an $h_{11/2}$ neutron hole to the 7^- core state [53]. According to the NSM calculations, the dominant configuration is 69% $\pi g^2_{7/2}\otimes\nu h^{-2}_{11/2}d^{-1}_{3/2}$ or 72% $|J_\pi = 0\rangle\otimes|J_\nu = 23/2\rangle$ of the $23/2^+_1$ state for ^{131}Te, and it is 56% $|J_\pi = 0\rangle\otimes|J_\nu = 23/2\rangle$ with 29% $|J_\pi = 2\rangle\otimes|J_\nu = 23/2\rangle$ mixing for ^{133}Xe [54]. Reference [11] also indicates that the $23/2^+_1$ states contain 81%, 60%, and 44% $\nu h^{-2}_{11/2}d^{-1}_{3/2}$ configurations or 72%, 54%, and 43% $|J_\pi = 0\rangle\otimes|J_\nu = 23/2\rangle$ configurations for ^{131}Te, ^{133}Xe, and ^{135}Ba, respectively.

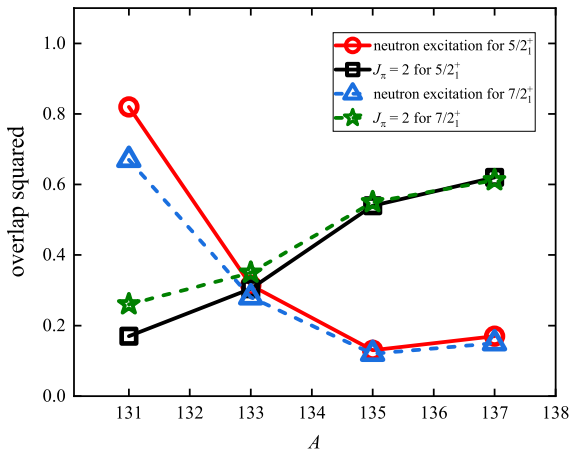

Fig. 5. (color online) Overlap squared between the neutron excitation and $|J_\pi = 2\rangle$ configurations with the wave functions of the $5/2^+_1$ and $7/2^+_1$ states versus the mass number A. The red circles (blue triangles) represent neutron excitation configurations for the $5/2^+_1$ ($7/2^+_1$) states, whereas the black squares (green stars) represent $|J_\pi = 2\rangle$ configurations for the $5/2^+_1$ ($7/2^+_1$) states.

The wave function of the $23/2^+_1$ state for ^{131}Te calculated using the NPA is

$$\left|23/2^+_1\right\rangle = |S^+_\pi\rangle\otimes[0.93|\mathcal{J}^-_\nu\otimes\nu h^{-1}_{11/2}\rangle - 0.92|I^-_\nu\otimes\nu h^{-1}_{11/2}\rangle - 0.92|\mathcal{A}^{(10)}_\nu\otimes\nu d^{-1}_{3/2}\rangle] + \cdots, \quad (24)$$

which is dominated by the neutron excitation configuration. Because neutron collective pairs with negative parity are primarily composed of $\nu h^{-1}_{11/2}d^{-1}_{3/2}$, the $\nu h^{-2}_{11/2}d^{-1}_{3/2}$ configuration plays an important role in the $23/2^+_1$ state, as presented in Fig. 4, which agrees closely with Refs. [3, 11, 53, 54].

The overlap squared between configurations $|J_\pi = 0\rangle$ and $|J_\pi = 2\rangle$ with the wave functions of the $23/2^+_1$ state versus the mass number A is plotted in Fig. 6, denoted by red circles and black squares, respectively. The $|J_\pi = 0\rangle$ ($|J_\pi = 2\rangle$) configuration decreases (increases) with A. The NPA calculations provide 87%, 67%, and 54% $|J_\pi = 0\rangle\otimes|J_\nu = 23/2\rangle$ configurations for ^{131}Te, ^{133}Xe, and ^{135}Ba, respectively, which are close to the results in Refs. [11, 54].

E. Negative parity states

For the $11/2^-_1$ and $15/2^-_1$ states ($21/2^-_1$ and $23/2^-_1$ states) of ^{131}Te and ^{133}Xe, the NSM calculations indicate that the dominant proton configurations are $|J_\pi = 0\rangle$ ($|J_\pi = 6\rangle$), whereas for the $19/2^-_1$ states, the dominant configurations are $|J_\pi = 4\rangle$ and $|J_\pi = 6\rangle$ [11, 54]. For ^{137}Ce, Ref. [55] suggests that the $11/2^-_1$ isomeric state is based on the $h_{11/2}$ neutron hole coupled to the even–even nuclear core, and the $15/2^-_1$ ($19/2^-_1$) state may be assigned the $\nu h^{-1}_{11/2}\otimes 2^+$ ($\nu h^{-1}_{11/2}\otimes 4^+$) multiplet.

The wave functions of the $11/2^-_1$ state for ^{131}Te, ^{133}Xe, ^{135}Ba, and ^{137}Ce in this paper are

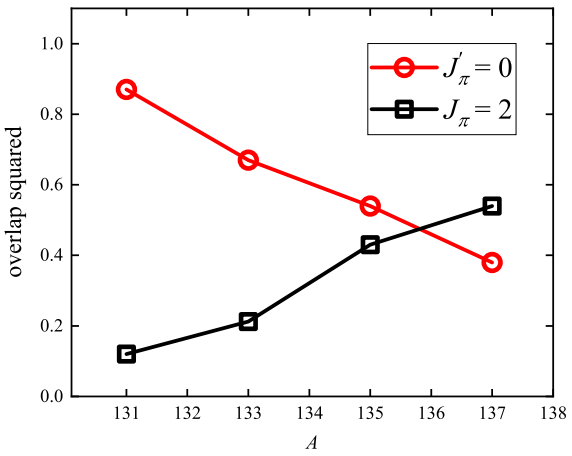

Fig. 6. (color online) Overlap squared between the configurations $|J_\pi = 0\rangle$ (red circles) and $|J_\pi = 2\rangle$ (black squares) with the wave functions of the $23/2^+_1$ state versus the mass number A.

$$
\begin{aligned}
\left|11/2_1^-\right\rangle &= 0.93|S_\pi^+\rangle\otimes|S_\nu^+\otimes\nu h_{11/2}^{-1}\rangle+\cdots,\\
\left|11/2_1^-\right\rangle &= 0.98|(S_\pi^+)^{N_\pi/2}\rangle\otimes|S_\nu^+\otimes\nu h_{11/2}^{-1}\rangle+\cdots,\\
\left|11/2_1^-\right\rangle &= 0.84|(S_\pi^+)^{N_\pi/2}\rangle\otimes|S_\nu^+\otimes\nu h_{11/2}^{-1}\rangle+\cdots,\\
\left|11/2_1^-\right\rangle &= 0.93|(S_\pi^+)^{N_\pi/2}\rangle\otimes|S_\nu^+\otimes\nu h_{11/2}^{-1}\rangle+\cdots,
\end{aligned}
\tag{25}
$$

respectively, which are all dominated by the neutron excitation configuration. The dominant components of $|S_\nu^+\otimes\nu h_{11/2}^{-1}\rangle$ configuration are $\nu h_{11/2}^{-3}$ and $\nu h_{11/2}^{-1}d_{3/2}^{-2}$; thus, the NPA calculations assign the $\nu h_{11/2}^{-3}$ configuration percentages as 55%, 53%, 41%, and 30%, and the $\nu h_{11/2}^{-1}d_{3/2}^{-2}$ configuration percentages as 38%, 36%, 48%, and 61% of the $11/2_1^-$ state for ^{131}Te, ^{133}Xe, ^{135}Ba, and ^{137}Ce, respectively.

In our NPA calculations, the wave functions of $13/2_1^-\sim 23/2_1^-$ and $27/2_1^-$ states for ^{131}Te are

$$
\begin{aligned}
|13/2_1^-\rangle =&0.74|S_\pi^+\rangle\otimes|D_\nu^+\otimes\nu h_{11/2}^{-1}\rangle\\
&+0.52|D_\pi^+\rangle\otimes|S_\nu^+\otimes\nu h_{11/2}^{-1}\rangle+\cdots,\\
|15/2_1^-\rangle =&0.82|S_\pi^+\rangle\otimes|D_\nu^+\otimes\nu h_{11/2}^{-1}\rangle\\
&+0.59|S_\pi^+\rangle\otimes|I_\nu^-\otimes\nu d_{3/2}^{-1}\rangle+\cdots,\\
|17/2_1^-\rangle =&-0.91|G_\pi^+\rangle\otimes|S_\nu^+\otimes\nu h_{11/2}^{-1}\rangle\\
&+0.57|G_\pi^+\rangle\otimes|\mathcal{A}_\nu^{(6)}\otimes\nu h_{11/2}^{-1}\rangle+\cdots,\\
|19/2_1^-\rangle =&-0.88|G_\pi^+\rangle\otimes|S_\nu^+\otimes\nu h_{11/2}^{-1}\rangle\\
&+0.58|G_\pi^+\rangle\otimes|\mathcal{A}_\nu^{(6)}\otimes\nu h_{11/2}^{-1}\rangle+\cdots,\\
|21/2_1^-\rangle =&0.79|I_\pi^+\rangle\otimes|S_\nu^+\otimes\nu h_{11/2}^{-1}\rangle+0.51|G_\pi^+\rangle\otimes|D_\nu^+\otimes\nu h_{11/2}^{-1}\rangle\\
&-0.50|I_\pi^+\rangle\otimes|\mathcal{A}_\nu^{(6)}\otimes\nu h_{11/2}^{-1}\rangle+\cdots,\\
|23/2_1^-\rangle =&-0.73|I_\pi^+\rangle\otimes|S_\nu^+\otimes\nu h_{11/2}^{-1}\rangle-0.61|G_\pi^+\rangle\otimes|D_\nu^+\otimes\nu h_{11/2}^{-1}\rangle\\
&+0.49|I_\pi^+\rangle\otimes|\mathcal{A}_\nu^{(6)}\otimes\nu h_{11/2}^{-1}\rangle+\cdots,\\
|27/2_1^-\rangle =&0.96|S_\pi^+\rangle\otimes|\mathcal{A}_\nu^{(10)}\otimes\nu h_{11/2}^{-1}\rangle\\
&-0.96|S_\pi^+\rangle\otimes|\mathcal{A}_\nu^{(8)}\otimes\nu h_{11/2}^{-1}\rangle+\cdots,
\end{aligned}
\tag{26}
$$

respectively, and $13/2_1^-$, $15/2_1^-$, and $27/2_1^-$ states are dominated by the neutron excitation. In addition, all these states exhibit a significant component of $\nu h_{11/2}^{-1}$.

The overlap squared between the neutron excitation and $|J_\pi=2\rangle$ configurations with the wave functions of the $13/2_1^-$ and $15/2_1^-$ states are plotted in Fig. 7 versus the mass number A. The red circles (blue triangles) and black squares (green stars) correspond to the neutron excitation configuration and $|J_\pi=2\rangle$ components for the $13/2_1^-$ ($15/2_1^-$) state, respectively. Both the $13/2_1^-$ and $15/2_1^-$ states of ^{131}Te are dominated by the neutron excitations, whereas those for ^{135}Ba and ^{137}Ce are dominated by the configuration $|J_\pi=2\rangle$.

Similar overlap squared between configurations $|J_\pi=4\rangle$ and $|J_\pi=2\rangle$ with the wave functions of the $17/2_1^-$ and $19/2_1^-$ states are presented in Fig. 8, and those between configurations $|J_\pi=6\rangle$ and the wave functions of the $21/2_1^-$ and $23/2_1^-$ states are presented in Fig. 9. The dominant component is $|J_\pi=4\rangle$ for $17/2_1^-$ and $19/2_1^-$ states of ^{131}Te and ^{133}Xe, $|J_\pi=2\rangle$ for $17/2_1^-$ states of ^{135}Ba and ^{137}Ce, and $|J_\pi=6\rangle$ of $21/2_1^-$ and $23/2_1^-$ states of ^{131}Te, ^{133}Xe, ^{135}Ba, and ^{137}Ce.

Energies of the Hamiltonian H_P and H_Q in single-j shells for an odd system with only one pair can be analytically obtained using the simplified Eqs. (30), (33), and (34) given in Appendix A. Thus, similar to Ref. [27], the configuration pictures of the $17/2_1^-$, $19/2_1^-$, $21/2_1^-$, and $23/2_1^-$ states for ^{131}Te can be understood from a simple perspective of single-j shells (protons in the $g_{7/2}$ orbit and neutron holes in the $h_{11/2}$ orbit). For valence protons, we consider the S_π^+ and G_π^+ (I_π^+) pairs in the $17/2_1^-$ and $19/2_1^-$ ($21/2_1^-$ and $23/2_1^-$) states, whereas for valence neutron holes, we consider $S_\nu^+\otimes\nu h_{11/2}^{-1}$ for all these four states, as well as $\mathcal{A}_\nu^{(4)}\otimes\nu h_{11/2}^{-1}$ ($\mathcal{A}_\nu^{(6)}\otimes\nu h_{11/2}^{-1}$) in the $17/2_1^-$ and $19/2_1^-$ ($21/2_1^-$ and $23/2_1^-$) states. The matrix elements of H_P and H_Q in single-j shells (and H_0 in many-j shells) are presented in Table 5.

According to Table 5, we have

$$
\begin{aligned}
\langle G_\pi^+\otimes S_\nu^+\otimes\nu h_{11/2}^{-1}|H|G_\pi^+\otimes S_\nu^+\otimes\nu h_{11/2}^{-1}\rangle &\approx -1.583\ \text{MeV},\\
\langle S_\pi^+\otimes(\mathcal{A}_\nu^{(4)}\otimes\nu h_{11/2}^{-1})_{J_\nu=17/2}|H|S_\pi^+\otimes(\mathcal{A}_\nu^{(4)}\otimes\nu h_{11/2}^{-1})_{J_\nu=17/2}\rangle &\approx -1.074\ \text{MeV},\\
\langle S_\pi^+\otimes(\mathcal{A}_\nu^{(4)}\otimes\nu h_{11/2}^{-1})_{J_\nu=19/2}|H|S_\pi^+\otimes(\mathcal{A}_\nu^{(4)}\otimes\nu h_{11/2}^{-1})_{J_\nu=19/2}\rangle &\approx -0.931\ \text{MeV}
\end{aligned}
\tag{27}
$$

for the $17/2_1^-$ and $19/2_1^-$ states, and

$$
\begin{aligned}
\langle I_\pi^+\otimes S_\nu^+\otimes\nu h_{11/2}^{-1}|H|I_\pi^+\otimes S_\nu^+\otimes\nu h_{11/2}^{-1}\rangle &\approx -1.599\ \text{MeV},\\
\langle S_\pi^+\otimes(\mathcal{A}_\nu^{(6)}\otimes\nu h_{11/2}^{-1})_{J_\nu=21/2}|H|S_\pi^+\otimes(\mathcal{A}_\nu^{(6)}\otimes\nu h_{11/2}^{-1})_{J_\nu=21/2}\rangle &\approx -0.757\ \text{MeV},\\
\langle S_\pi^+\otimes(\mathcal{A}_\nu^{(6)}\otimes\nu h_{11/2}^{-1})_{J_\nu=23/2}|H|S_\pi^+\otimes(\mathcal{A}_\nu^{(6)}\otimes\nu h_{11/2}^{-1})_{J_\nu=23/2}\rangle &\approx -0.710\ \text{MeV}
\end{aligned}
\tag{28}
$$

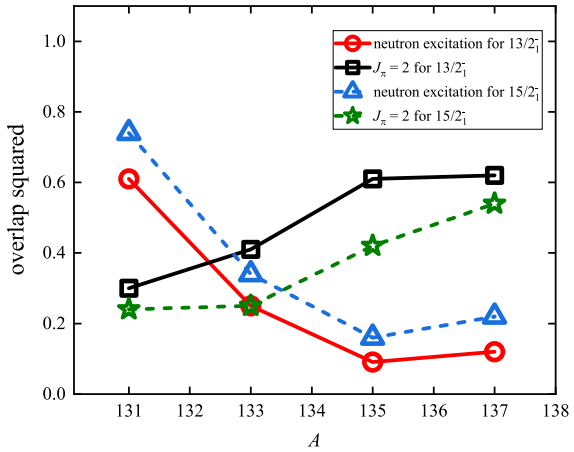

Fig. 7. (color online) Overlap squared between the neutron excitation and $|J_\pi = 2\rangle$ configurations with the wave functions of the $13/2_1^-$ and $15/2_1^-$ states versus the mass number A. The red circles and black squares correspond to the neutron excitation configuration and $|J_\pi = 2\rangle$ components for the $13/2_1^-$ state, respectively. The blue triangles and green stars correspond to the neutron excitation configuration and $|J_\pi = 2\rangle$ components for the $15/2_1^-$ state, respectively.

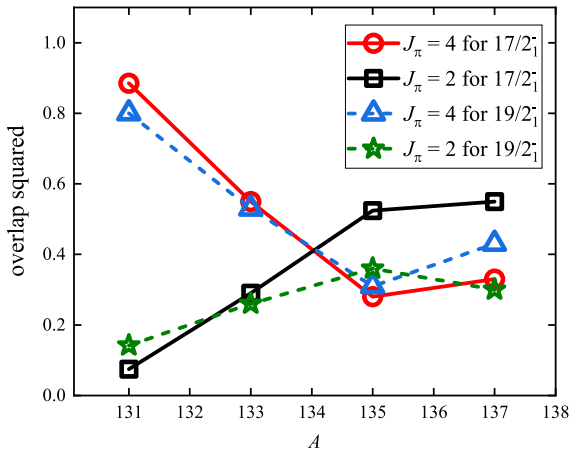

Fig. 8. (color online) Overlap squared between configurations $|J_\pi = 4\rangle$ and $|J_\pi = 2\rangle$ with the wave functions of the $17/2_1^-$ and $19/2_1^-$ states versus the mass number A. The red circles and black squares correspond to configurations $|J_\pi = 4\rangle$ and $|J_\pi = 2\rangle$ for the $17/2_1^-$ state. The blue triangles and green stars correspond to configurations $|J_\pi = 4\rangle$ and $|J_\pi = 2\rangle$ for the $19/2_1^-$ state.

for the $21/2_1^-$ and $23/2_1^-$ states. The energies of neutron excitation configurations are much larger than those of $G_\pi^+ \otimes S_\nu^+ \otimes \nu h_{11/2}^{-1}$ and $I_\pi^+ \otimes S_\nu^+ \otimes \nu h_{11/2}^{-1}$. Thus, the $17/2_1^-$ and $19/2_1^-$ ($21/2_1^-$ and $23/2_1^-$) states of ^{131}Te are dominated by configuration $G_\pi^+ \otimes S_\nu^+ \otimes \nu h_{11/2}^{-1}$ ($I_\pi^+ \otimes S_\nu^+ \otimes \nu h_{11/2}^{-1}$), which is consistent with Eq. (26). This indicates that the $17/2_1^-$ and $19/2_1^-$ ($21/2_1^-$ and $23/2_1^-$) states of ^{131}Te can be described as consisting of the 4_1^+ (6_1^+) states of ^{132}Te, which is suggested to be dominated by proton excitations $G_\pi^+ \otimes S_\nu^+$ ($I_\pi^+ \otimes S_\nu^+$) in Ref. [27], coupled with a neutron hole occupies the $h_{11/2}$ orbit.

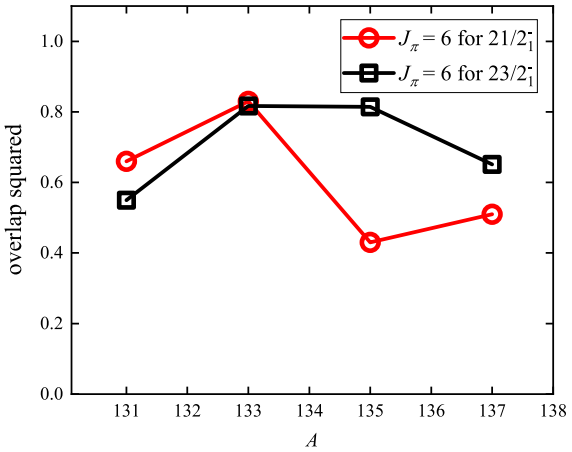

Fig. 9. (color online) Overlap squared between configurations $|J_\pi = 6\rangle$ and the wave functions of the $21/2_1^-$ and $23/2_1^-$ states versus the mass number A. The red circles and black squares correspond to configurations $|J_\pi = 6\rangle$ for the $21/2_1^-$ and $23/2_1^-$ states, respectively.

IV. SUMMARY

In this paper, we study the low-lying states of five odd-A nuclei with neutron number $N = 79$, *i.e.*, ^{129}Sn, ^{131}Te, ^{133}Xe, ^{135}Ba, and ^{137}Ce, within NPA. Low-lying energy spectra for these nuclei with both positive and negative parities, as well as $B(E2)$ transition rates and g factors of these low-lying states, are calculated. Most of them agree closely with experimental data. Some of the unknown $B(E2)$ and g factors are predicted based on the NPA wave functions obtained in this paper.

The wave functions of some low-lying states of these nuclei are discussed in detail, and the NPA calculations show that many of these states have a simple structure in the nucleon-pair basis. The neutron part of the $1/2_1^+$ states of these five nuclei is dominated by the configuration $|S_\nu^+ \otimes \nu s_{1/2}^{-1}\rangle$. The dominant components of the $5/2_1^+$ and $7/2_1^+$ states for ^{129}Sn and ^{131}Te are the neutron excitation configuration $|D_\nu^+ \otimes \nu d_{3/2}^{-1}\rangle$, whereas that for ^{135}Ba and ^{137}Ce is $|J_\pi = 2\rangle$. The $23/2_1^+$ state is primarily composed of $\nu h_{11/2}^{-2} d_{3/2}^{1}$ coupled with $|J_\pi = 0\rangle$ for ^{129}Sn, ^{131}Te, and ^{133}Xe. For the negative parity $11/2_1^-$ states of these five nuclei, the dominant neutron configuration is $|S_\nu^+ \otimes \nu h_{11/2}^{-1}\rangle$. The $13/2_1^-$, $15/2_1^-$, and $27/2_1^-$ states of ^{131}Te are dominated by the neutron excitation, and the configurations of the $17/2_1^-$, $19/2_1^-$, $21/2_1^-$, and $23/2_1^-$ states for ^{131}Te are analyzed in single-j shells.

In combination with the previous NPA calculations of even-even $N = 80$ isotones [27], we show that the NPA is an efficient and convenient method for studying the struc-

Table 5. Matrix elements (in MeV) of H_0, V_0, V_2, V_4, and V_Q for a few configurations of ^{131}Te with the phenomenological NSM Hamiltonian. The matrix elements of single-particle energies H_0 are calculated in many-j shells. The results of V_0, V_2, V_4, and V_Q are for single-j shells with valence protons in the $g_{7/2}$ orbit and valence neutron holes in the $h_{11/2}$ orbit; these matrix elements are derived analytically using Eqs. (30), (33), and (34) in Appendix A. Both V_{10} and $V_{Q_{\pi\nu}}$ equal zero in these configurations with such single-j shells and are not listed here.

^{131}Te	H_0	$-V_0$	$-V_2$	$-V_4$	$-V_Q$
$S^+_\nu \otimes \nu h^{-1}_{11/2}$	0.422	$\frac{553}{500}$	0	0	$\frac{677}{313\pi}$
$(\mathcal{A}^{(4)}_\nu \otimes \nu h^{-1}_{11/2})_{J_\nu=17/2}$	0.109	0	< 0.001	$\frac{388}{785\pi}$	$\frac{1629}{1010\pi}$
$(\mathcal{A}^{(4)}_\nu \otimes \nu h^{-1}_{11/2})_{J_\nu=19/2}$	0.089	0	< 0.001	$\frac{1038}{3079\pi}$	$\frac{801}{637\pi}$
$(\mathcal{A}^{(6)}_\nu \otimes \nu h^{-1}_{11/2})_{J_\nu=21/2}$	0.170	0	< 0.001	< 0.001	$\frac{2540}{1953\pi}$
$(\mathcal{A}^{(6)}_\nu \otimes \nu h^{-1}_{11/2})_{J_\nu=23/2}$	0.097	0	< 0.001	< 0.001	$\frac{989}{1070\pi}$
S^+_π	0.925	$\frac{21}{28}$	0	0	$\frac{121}{56\pi}$
G^+_π	0.199	0	0	$\frac{667}{1175\pi}$	$\frac{121}{168\pi}$
I^+_π	0.003	0	0	0	$\frac{121}{168\pi}$

ture for nuclei with $A \sim 130$. The simple structure of the low-lying states within the nucleon-pair basis appears in both even-even and odd-A nuclei. Therefore, an interesting aspect to explore is whether a similar phenomenon exists in odd-odd nuclei, and this can be discussed in the future.

APPENDIX A: OVERLAPS AND MATRIX ELEMENTS OF THE HAMILTONIAN FOR ONE PAIR IN ODD SYSTEMS

In this Appendix, we present the expressions of the overlaps and matrix elements of $P^{(s)\dagger}\cdot P^{(s)}$ and $Q^{(t)}\cdot Q^{(t)}$ for odd systems based on Ref. [30].

A.1. Overlaps

According to Eq. (6.2) in Ref. [30], the overlap for one pair in an odd system is

$$\begin{aligned}\langle j'_0 s_1; J_1 | j_0 r_1; J_1\rangle &= 2\delta_{s_1 r_1}\delta_{j_0 j'_0}\sum_{ab} y(abs_1)y(abr_1)\\ &+ 4\hat{r}_1\hat{s}_1\sum_{j'} y(j' j'_0 r_1)y(j' j_0 s_1)\begin{Bmatrix} r_1 & j'_0 & j'\\ s_1 & j_0 & J_1\end{Bmatrix},\end{aligned} \tag{A1}$$

where $\hat{r}=\sqrt{2r+1}$, and "{ }" denotes the 6j symbol. For nucleons in a single-j shell, Eq. (29) can be further simplified to

$$\begin{aligned}\langle j s_1; J_1 | j r_1; J_1\rangle &= 2\delta_{s_1 r_1} y(jjs_1)y\\ &+ 4\hat{r}_1\hat{s}_1 y(jjr_1)y(jjs_1)\begin{Bmatrix} r_1 & j & j\\ s_1 & j & J_1\end{Bmatrix}.\end{aligned} \tag{A2}$$

A.2. Matrix elements of $P^{(s)\dagger}\cdot P^{(s)}$

According to Eq. (6.5) in Ref. [30], the matrix elements of $P^{(s)\dagger}\cdot P^{(s)}$ for one pair in an odd system is

$$\begin{aligned}\langle j'_0 r_1; J_1 | P^{(s)\dagger}\cdot P^{(s)} | j_0 s_1; J_1\rangle &= \phi_0\hat{s}\delta_{sr_1}\langle j'_0 s; J_1 | j_0 s_1; J_1\rangle\\ &+ 4\sum_{tj'b}(-1)^{t-s-r_1}\frac{\hat{s}}{\hat{j}'}(2t+1)U(j'_0 t J_1 s; j' r_1)y(j' b r_1)y_0(b j'_0 s)\\ &\times\begin{Bmatrix} r_1 & s & t\\ j'_0 & j' & b\end{Bmatrix}\langle j' s; J_1 | j_0 s_1; J_1\rangle,\end{aligned} \tag{A3}$$

where $U(abcd;ef)$ is a unitary Racha coefficient,

$$\phi_0 = \frac{2}{\hat{s}}\sum_{ab} y(abs)y_0(abs), \tag{A4}$$

and $y_0(abs)$ is the pair structure coefficient of $P^{(s)\dagger}$. For nucleons in a single-j shell, Eq. (31) can be further simplified to

$$\begin{aligned}\langle jr_1;J_1|P^{(s)\dagger}\cdot P^{(s)}|js_1;J_1\rangle &= 2y(jjs)y_0(jjs)\delta_{sr_1}\langle js;J_1|js_1;J_1\rangle\\ &+4\sum_t(-1)^{t-s-r_1}\frac{\hat{s}}{\hat{j}}(2t+1)U(jtJ_1s;jr_1)y(jjr_1)y_0(jjs)\\ &\times\begin{Bmatrix} r_1 & s & t\\ j & j & j\end{Bmatrix}\langle js;J_1|js_1;J_1\rangle,\end{aligned} \tag{A5}$$

where $\langle js;J_1|js_1;J_1\rangle$ is given by Eq. (30) with r_1 replaced by s and $y(jjr_1)$ replaced by $y_0(jjs)$.

A.3. Matrix elements of $Q^{(t)}\cdot Q^{(t)}$

According to Eq. (6.4) in Ref. [30], the matrix elements of $Q^{(t)}\cdot Q^{(t)}$ for one pair in an odd system is

$$\begin{aligned}\langle j_0'r_1;J_1|Q^{(t)}\cdot Q^{(t)}|j_0s_1;J_1\rangle &= \sum_{r_1'}(-1)^{r_1'-r_1-t}\frac{\hat{r}_1'}{\hat{r}_1}\langle j_0'(r_1)_{\mathbf{B}};\\ &J_1|j_0s_1;J_1\rangle+\sum_{j'}\frac{2t+1}{2j_0'+1}q(j_0'j't)^2\langle j_0'r_1;J_1|j_0s_1;J_1\rangle\\ &-2\sum_{r_1'j'}\frac{\hat{r}_1'\hat{t}}{\hat{r}_1\hat{j}'}U(j_0'tJ_1r_1';j'r_1)q(j'j_0't)\langle j'(\mathbf{r}_1');J_1|j_0s_1;J_1\rangle,\end{aligned} \tag{A6}$$

where $(r_1)_{\mathbf{B}}\equiv\tilde{\mathbf{B}}^{r_1}(r_1')$ is defined as

$$\begin{aligned}\tilde{\mathbf{B}}^{r_k}(r_k') &= [[\tilde{A}^{r_k},Q^{(t)}]^{(r_k')},Q^{(t)}]=\sum_{ab}\bar{y}(abr_k)\tilde{A}^{r_k}(ab),\\ \bar{y}(abr_k) &= \bar{z}(abr_k)-(-1)^{a+b+r_k}\bar{z}(abr_k),\\ \bar{z}(abr_k) &= 2\hat{r_k'}\hat{r}_k(2t+1)\sum_{dd'}y(dd'r_k)q(d'bt)\\ &q(dat)\begin{Bmatrix} r_k & t & r_k'\\ b & d & d'\end{Bmatrix}\begin{Bmatrix} r_k & t & r_k'\\ d & b & a\end{Bmatrix},\end{aligned} \tag{A7}$$

and $(\mathbf{r}_1')\equiv\tilde{\mathcal{A}}^{r_1'}$ is defined as

$$\begin{aligned}\tilde{\mathcal{A}}^{r_k'} &= [\tilde{A}^{r_k},Q^{(t)}]^{(r_k')}=\sum_{ad}y'(dar_k')\tilde{A}^{r_k'}(da),\\ y'(dar_k') &= z(dar_k')-(-1)^{d+a+r_k'}z(adr_k'),\\ z(dar_k') &= \hat{r}_k\hat{t}\sum_{b_k}y(ab_kr_k)q(b_kdt)\begin{Bmatrix} r_k & t & r_k'\\ d & a & b_k\end{Bmatrix}\end{aligned} \tag{A8}$$

with $k=1$. For nucleons in a single-j shell with $t=2$, Eq. (34) can be further simplified to

$$\begin{aligned}\langle jr_1;J_1|Q^{(2)}\cdot Q^{(2)}|js_1;J_1\rangle &= \sum_{r_1'}(-1)^{r_1'-r_1}\frac{\hat{r}_1'}{\hat{r}_1}\langle j(r_1)_{\mathbf{B}};J_1|js_1;J_1\rangle\\ &+\frac{5}{2j+1}q(jj2)^2\langle jr_1;J_1|js_1;J_1\rangle\\ &-2\sqrt{5}\sum_{r_1'}\frac{\hat{r}_1'}{\hat{r}_1\hat{j}}U(j2J_1r_1';jr_1)q(jj2)\langle j(\mathbf{r}_1');J_1|js_1;J_1\rangle,\end{aligned} \tag{A9}$$

where $\langle jr_1;J_1|js_1;J_1\rangle$ is given by Eq. (30), and

$$\begin{aligned}\langle j(r_1)_{\mathbf{B}};J_1|js_1;J_1\rangle &= 2\delta_{s_1r_1}y(jjs_1)\bar{y}(jjr_1)\\ &+4\hat{r}_1\hat{s}_1\bar{y}(jjr_1)y(jjs_1)\begin{Bmatrix} s_1 & j & j\\ r_1 & j & J_1\end{Bmatrix},\\ \langle j(\mathbf{r}_1');J_1|js_1;J_1\rangle &= 2\delta_{s_1r_1'}y(jjs_1)y'(jjr_1')\\ &+4\hat{r}_1'\hat{s}_1y'(jjr_1')y(jjs_1)\begin{Bmatrix} s_1 & j & j\\ r_1' & j & J_1\end{Bmatrix},\end{aligned} \tag{A10}$$

with

$$\begin{aligned}\bar{y}(jjr_1) &= 20\hat{r}_1\hat{r}_1'y(jjr_1)[q(jj2)]^2\begin{Bmatrix} r_1 & 2 & r_1'\\ j & j & j\end{Bmatrix}^2,\\ y'(jjr_1) &= 2\sqrt{5}\hat{r}_1y(jjr_1)q(jj2)\begin{Bmatrix} r_1 & 2 & r_1'\\ j & j & j\end{Bmatrix}.\end{aligned} \tag{A11}$$

References

[1] R. Lozeva, G. Simpson, G. Neyens *et al.*, AIP Conf. Proc. **1090**, 164 (2009)
[2] S. Kaim, A. Aboudi, R. Belgharbi *et al.*, Cumhuriyet Sci. J. **39**, 118 (2018)
[3] H. K. Wang, S. K. Ghorui, Z. Q. Chen *et al.*, Phys. Rev. C **102**, 054316 (2020)
[4] R. E. Chrien, B. K. S. Koene, M. L. Stelts *et al.*, Phys. Rev. C **48**, 109 (1993)
[5] K. Nomura, R. Rodríguez-Guzmán, and L. M. Robledo, Phys. Rev. C **101**, 024311 (2020)
[6] M. P. Kartamyshev, T. Engeland, M. Hjorth-Jensen *et al.*, Phys. Rev. C **76**, 024313 (2007)
[7] N. Yoshinaga, K. Higashiyama, R. Arai *et al.*, Phys. Rev. C **87**, 044332 (2013)
[8] N. Yoshinaga, K. Higashiyama, R. Arai *et al.*, Phys. Rev. C **89**, 069902 (2014)
[9] E. Teruya, N. Yoshinaga, K. Higashiyama *et al.*, Phys. Rev. C **92**, 034320 (2015)
[10] A. J. Majarshin, Y. A. Luo, F. Pan *et al.*, J. Phys. G: Nucl. Part. Phys. **48**, 125107 (2021)

[11] L. Kaya, A. Vogt, P. Reiter *et al*., Phys. Rev. C **98**, 054312 (2018)
[12] M. G. Mayer, Phys. Rev. **74**, 235 (1948)
[13] M. G. Mayer, Phys. Rev. **75**, 1969 (1949)
[14] M. G. Mayer, Phys. Rev. **78**, 16 (1950)
[15] S. Koonin, D. Dean, and K. Langanke, Phys. Rep. **278**, 1 (1997)
[16] T. Otsuka, M. Honma, T. Mizusaki *et al*., Prog. Part. Nucl. Phys. **47**, 319 (2001)
[17] E. Caurier, G. Martínez-Pinedo, F. Nowacki *et al*., Rev. Mod. Phys. **77**, 427 (2005)
[18] Y. M. Zhao, S. Yamaji, N. Yoshinaga *et al*., Phys. Rev. C **62**, 014315 (2000)
[19] Y. M. Zhao, S. Yamaji, N. Yoshinaga *et al*., Phys. Rev. C **62**, 014316 (2000)
[20] Y. M. Zhao, S. Yamaji, N. Yoshinaga *et al*., Phys. Rev. C **62**, 024322 (2000)
[21] Y. Zhao and A. Arima, Phys. Rep. **545**, 1 (2014)
[22] Y. Y. Zong, C. Ma, H. Jiang *et al*., Phys. Rev. C **109**, 064306 (2024)
[23] L. Y. Jia, H. Zhang, and Y. M. Zhao, Phys. Rev. C **75**, 034307 (2007)
[24] L. Y. Jia, H. Zhang, and Y. M. Zhao, Phys. Rev. C **76**, 054305 (2007)
[25] Y. Lei, Y. M. Zhao, and A. Arima, Phys. Rev. C **84**, 044301 (2011)
[26] Y. Y. Cheng, Y. Lei, Y. M. Zhao *et al*., Phys. Rev. C **92**, 064320 (2015)
[27] M. Bao, H. Jiang, Y. M. Zhao *et al*., Phys. Rev. C **101**, 014316 (2020)
[28] H. Jiang, C. H. Mao, Y. Lei *et al*., Phys. Rev. C **110**, 014315 (2024)
[29] J. Q. Chen, Nucl. Phys. A **626**, 686 (1997)
[30] Y. M. Zhao, N. Yoshinaga, S. Yamaji *et al*., Phys. Rev. C **62**, 014304 (2000)
[31] G. J. Fu, Y. Lei, Y. M. Zhao *et al*., Phys. Rev. C **87**, 044310 (2013)
[32] Y. Y. Cheng, Y. M. Zhao, and A. Arima, Phys. Rev. C **97**, 024303 (2018)
[33] C. Ma, X. Yin, and Y. M. Zhao, Phys. Rev. C **108**, 034308 (2023)
[34] B. Fogelberg and J. Blomqvist, Nucl. Phys. A **429**, 205 (1984)
[35] W. J. Baldridge, Phys. Rev. C **18**, 530 (1978)
[36] Ensdf viewer, National Nuclear Data Center https://www.nndc.bnl.gov/
[37] Y. Lei, Z. Y. Xu, Y. M. Zhao *et al*., Phys. Rev. C **80**, 064316 (2009)
[38] R. L. Lozeva, G. S. Simpson, H. Grawe *et al*., Phys. Rev. C **77**, 064313 (2008)
[39] D. Kumar, A. Pal, S. Basak *et al*., Phys. Rev. C **109**, 024304 (2024)
[40] K. Higashiyama and N. Yoshinaga, Phys. Rev. C **83**, 034321 (2011)
[41] H. Jiang, Y. Lei, C. Qi *et al*., Phys. Rev. C **89**, 014320 (2014)
[42] Z. W. Li, B. C. He, L. Li *et al*., Int. J. Mod. Phys. E **31**, 2250014 (2022)
[43] H. K. Wang, K. Kaneko, Y. Sun *et al*., Phys. Rev. C **95**, 011304 (2017)
[44] H. Gausemel, B. Fogelberg, T. Engeland *et al*., Phys. Rev. C **69**, 054307 (2004)
[45] A. Holt, T. Engeland, M. Hjorth-Jensen *et al*., Nucl. Phys. A **634**, 41 (1998)
[46] R. Lică, H. Mach, L. M. Fraile *et al*., Phys. Rev. C **93**, 044303 (2016)
[47] J. Genevey, J. A. Pinston, C. Foin *et al*., Phys. Rev. C **65**, 034322 (2002)
[48] Ł. W. Iskra, R. Broda1, R. V. F. Janssens *et al*., Phys. Rev. C **93**, 014303 (2016)
[49] I. Tomandl, T. von Egidy, J. Honzátko *et al*., Nucl. Phys. A **717**, 149 (2003)
[50] J. Blachot, H. N. Erten, C. D. Coryell *et al*., Phys. Rev. C **4**, 214 (1971)
[51] M. A. M. Shahabuddin, J. A. Kuehner, and A. A. Pilt, Phys. Rev. C **23**, 64 (1981)
[52] H. K. Wang, S. K. Ghorui, K. Kaneko *et al*., Phys. Rev. C **96**, 054313 (2017)
[53] B. Fogelberg, H. Mach, H. Gausemel *et al*., AIP Conf. Proc. **447**, 191 (1998)
[54] A. Vogt, M. Siciliano, B. Birkenbach *et al*., Phys. Rev. C **96**, 024321 (2017)
[55] R. Palit, M. S. R. Laskar, S. Nag *et al*., Eur. Phys. J. ST **233**, 933 (2024)